Pergamon

PII: S0306-4522(01)00043-4

www.elsevier.com/locate/neuroscience

Neuroscience Vol. 104, No. 2, pp. 379–396, 2001

0306-4522/01 $20.00+0.00

ENHANCED BUT FRAGILE INHIBITION IN THE DENTATE GYRUS *IN VIVO* IN THE KAINIC ACID MODEL OF TEMPORAL LOBE EPILEPSY: A STUDY USING CURRENT SOURCE DENSITY ANALYSIS

K. WU and L. S. LEUNG*

Departments of Clinical Neurological Sciences and Physiology, University of Western Ontario, London, Ontario, Canada N6A 5A5

Abstract—Temporal lobe epilepsy is related to many structural and physiological changes in the brain. We used kainic acid in rats as an animal model of temporal lobe epilepsy, and studied the neural interactions of the dentate gyrus in urethane-anesthetized rats *in vivo*. Our initial hypothesis was that sprouting of mossy fibers, the axons of the granule cells, increases proximal dendritic excitatory currents in the inner molecular layer of the dentate gyrus. Extracellular currents were detected *in vivo* using current source density analysis. Backfiring the mossy fibers in CA3 or orthodromic excitation of the granule cells through the medial perforant path induced a current sink at the inner molecular layer. However, the sink or inferred excitation at the inner molecular layer was not increased in kainic acid-treated rats and the sink actually correlated negatively with the degree of mossy fiber sprouting. It is inferred that the latter sink was mediated mainly by association fibers and not by recurrent mossy fibers. After kainic acid treatment, paired–pulse inhibition of the population spikes in the dentate gyrus was increased. In contrast, reverberant activity that involved looping around an entorhinal–hippocampal circuit was increased in kainic acid-treated rats, compared to control rats. The increase of inhibition in kainic acid-treated rats was readily blocked by a small dose of $GABA_A$ receptor antagonist bicuculline. The latter dose of bicuculline induced paroxsymal spike bursts in kainic acid-treated but not control rats, demonstrating that the increased inhibition in dentate gyrus was fragile.

In conclusion, after kainic acid induced seizures, the dentate gyrus *in vivo* showed an increase in inhibition that appeared to be fragile. The hypothesized increase in proximal dendritic excitation due to mossy fiber sprouting was not detected. However, the fragile inhibition could explain the seizure susceptibility in patients with temporal lobe epilepsy.

Key words: mossy fibers, sprouting, seizures, CA3, recurrent excitation, population spikes.

Temporal lobe epilepsy (TLE) in humans is often accompanied by prominent neuropathology such as cell loss and mossy fiber sprouting (MFS).[2,21,31,43,59] It is unclear whether MFS causes further functional changes or increases seizure susceptibility. Previous studies suggest that MFS mediates recurrent excitation and enhances action potential bursts among granule cells in the dentate gyrus (DG).[8,18,43,50,61,68,2,18,43,61] The recurrent excitation mediated by MFS after seizures may normally be masked by recurrent inhibition.[8,18,50,68] In contrast, it has also been suggested that the sprouted mossy fibers may increase inhibition by synapsing on inhibitory interneurons in the inner molecular layer (IML) of the DG and in the hilus.[24,34,57] Electrophysiological studies in different animal models of TLE[7,9,14,29,45,49,63] or in human TLE[23,32,60,65] typically showed an increase in inhibition in the DG, although there were also reports to the contrary.[5,56,64] There is evidence that seizures induce a change in the composition of the $GABA_A$ receptor[7], such that the receptor may respond differently to benzodiazepine or Zn^{2+} after seizures.[7,14]

The main goal of this study was to investigate how synaptic transmission in the DG was altered at a long time (two to four months) after kainic acid (KA) injection. KA induced limbic seizures and resulted in pathology in rats that was similar to that in TLE in humans, including cell loss and MFS.[8,18,48,50,61,68] The DG is a main gateway into the hippocampus[15,40] and it has been suggested to gate seizures as well.[30,41] A major afferent of the DG is the medial perforant path (MPP) derived from the medial entorhinal cortex,[39,40] while CA3 provides an important recurrent feedback.[1,66] Both MPP and CA3 were stimulated in this study, and the field potentials were mapped in the DG. Current source density (CSD) analysis was used to reveal the macroscopic currents mediated by functional synapses at a particular layer in the DG.[36,47]

*Corresponding author. Tel: +1-519-663-3733; fax: +1-519-661-3753.

E-mail address: sleung@julian.uwo.ca (L. S. Leung).

Abbreviations: aCSF, artificial cerebrospinal fluid; ANCOVA, analysis of covariance; ANOVA, analysis of variance; CA, Cornu Ammonis; CSD, current source density; DG, dentate gyrus; EPSP, excitatory postsynaptic potential; GC, granule cell; GCL, granule cell layer; IML, inner molecular layer of the dentate gyrus; IPI, interpulse interval; IPSP, inhibitory postsynaptic potential; KA, kainic acid; MFS, mossy fiber sprouting; MML, middle molecular layer of the dentate gyrus; MPP, medial perforant path; NMDA, *N*-methyl-D-aspartate; OD, optical density; OML, outer molecular layer of the dentate gyrus; PS, population spike; TLE, temporal lobe epilepsy.

Other than comparing the field synaptic currents induced by various inputs to the DG, in particular, we reasoned that MFS may result in recurrent excitation in the IML that should be revealed using CSD analysis. Excitation of the granule cells at the IML would result in an inward current or current sink in the IML accompanied by outward currents in other parts of the granule cells. Thus, we initially hypothesized that MFS in KA-treated rats would be accompanied by an increase in an IML sink following orthodromic and antidromic activation of the dentate granule cells. In addition, we also studied how the paired–pulse inhibition in the DG may be affected by different degrees of inhibitory blockade using a $GABA_A$ receptor antagonist.

EXPERIMENTAL PROCEDURES

This project was concerned with the change in the brain *in vivo* after experimental seizures, and it could not be carried out using only *in vitro* preparations. Experimental procedures with animals were approved by the University Animal Use Committee. All efforts were made to minimize the number of animals used and their suffering.

Kainic acid injection

Male hooded (Long–Evans) rats (50–60 days old) were injected with KA (Sigma, St. Louis, MO) i.c.v. at 1 mm posterior (P) to bregma, 1.4 mm lateral (L) to the midline, and 4.2–4.4 mm ventral to the skull surface under sodium pentobarbital (60 mg/kg, i.p.) anesthesia. KA was injected (0.5 μg in 1 μl volume of artificial cerebrospinal fluid; aCSF) over a 10 min period per side and the injection needle was left in place for another 2 min. Both unilateral ($n = 17$) and bilateral ($n = 14$) injections were performed. The seizures were monitored for at least 6 h after injection. Control animals were injected with aCSF or saline.

Electrophysiology after kainic acid or control treatment

Two to four months after injection, rats were anesthetized with urethane (1.2–1.3 g/kg, i.p.) and positioned in a stereotaxic apparatus. The surgical, stimulation, recording, and analysis procedures were similar to those used in a previous report.[66] The stimulating and recording electrodes were placed on the same side that KA was injected, whether the injection was unilateral or bilateral. Stimulating electrodes (125 μm Teflon-insulated steel wires) were placed at: (i) the MPP: P 8, L 4.4, D 3.0–3.3 (D = depth below the skull surface) to orthodromically activate the DG (Fig. 1A); and (ii) CA3b: P 3.2, L 3.2 and D 3.6–4.0 mm to antidromically stimulate the mossy fibers (Fig. 1B). However, as shown previously,[66] CA3b stimulation also excited the DG and CA3c (Fig. 1B). The depth of the stimulus electrode was optimized by small steps (≤0.1 mm) in order to evoke the largest responses. Photo-isolated constant current pulses of 0.2 ms duration were delivered cathodally to one of the two sites at a repetition rate <0.15 Hz. A screw in the frontal skull served as the stimulus anode.

The field potentials were recorded in dorsal hippocampus at P 3.2–4.0, L 2.2–2.6 using either a glass micropipette or a16-channel silicon probe. The glass micropipette filled with 2 M sodium acetate and 4% pontamine sky blue (5–15 MΩ) was mounted on a Burleigh microdrive (1 μm step resolution) and lowered in a track that passed through CA1 and DG. The field potentials were amplified and bandpass filtered between 0.1 Hz (6 dB/octave roll off to low frequency) and 2 kHz (12 dB/octave roll off to high frequency). The evoked potentials were digitized at 10 kHz and averaged (eight sweeps) using a custom program on a microcomputer. At the granule cell and middle molecular layers of the DG, the input/output profiles were recorded following paired–pulse stimulation of MPP or CA3, using various intensities (10–600 μA) and interpulse intervals (IPIs; 10–200 ms). An automated laminar profile of average evoked potentials was then recorded sequentially, in a deep-to-surface direction. At one depth, responses to two stimulation sites (CA3 and MPP) were recorded before moving up to the next recording depth. Paired–pulses of 200 μA intensity (see Results for justification) and 50 ms IPI were delivered to each stimulus site. A profile at 50-μm depth intervals and spanning ~1 mm (from the ventral to dorsal blade of the DG) took about 60 min. Average responses were also recorded at a non-moving glass electrode in the DG during the mapping, and deviations of the average peak response of <10% from the grand mean was considered an acceptable level of stationarity.

The silicon probes were kindly provided by the NIH Center for Communications Technology, University of Michigan. The probe used had 16 recording pads separated by 100 μm on a vertical shank. It was lowered vertically into the DG and its position was optimized based on the evoked responses. The field potentials were amplified by a two-stage amplifier (AC Instrumentation Inc, Seattle, WA). Following a high pass (0.08 Hz) filter, the 16 channels were simultaneously recorded by means of 16 sample-and-hold circuits and digitized at 20 kHz. Single or average (typical four) sweeps of evoked potentials were stored in a microcomputer using a custom program.

Drug administration

The $GABA_A$ receptor antagonist bicuculline methiodide (sigma) was injected at two doses i.c.v. Seven control and eight KA-treated rats were given 1.5 μl of 5 mM bicuculline in aCSF. For simplicity of description, we refer to the latter as the low dose of bicuculline. Six control and four KA-treated rats were given 1.5 μl of 20 mM bicuculline in aCSF, which we will refer to as the high dose of bicuculline. The field potentials were recorded using the 16-channel silicon probe before and after bicuculline injection.

Data analysis

CSDs were calculated in one (z-) dimension, assuming that currents in the x- and y- directions were negligible, using the formula[25,36,37,47]

$$CSD(z) = \left[\frac{[2\phi(z) - \phi(z + 2\Delta z) - \phi(z - 2\Delta z)]}{(2\Delta z)^2} \right] \sigma_z$$

where CSD(z) is the current-source-density at depth z, $\phi(z)$ is the average evoked potential at depth z, Δz is the depth interval (typically 50 μm for glass pipette recording, 100 μm for 16-channel probe recording), and σ_z is the conductivity in the z-direction, assumed homogeneous. CSDs were calculated in units of mV/mm,^{2} proportional to the actual current densities. All values of CSD should be multiplied by the conductivity (σ_z) to give actual current densities. Pilot studies in normal or KA-treated rats showed similar CSD depth patterns for the IML sink (or any other events) mapped at Δz of 25 or 50 μm, suggesting that mapping at 50-μm intervals was adequate for CSD analysis of the IML or other sinks such as the middle molecular layer (MML).

The onset latency and the peak amplitude of the maximal sink in various layers of the DG were measured. The slope of the late MML sink was measured before the onset of the late population spike (PS). Input/output curves were constructed from the average field potentials recorded by the 16-channel probes. Excitatory postsynaptic potential (EPSP) slope was measured at MML in a 1.5–2-ms time window (starting from 0.2–0.4 ms after EPSP onset and ending 1.5–2 ms later, at least 0.2 ms before the onset of a population spike). The paired–pulse ratio of EPSP slope was estimated as the ratio of the slope of the second (EPSP2) to the first (EPSP1), following paired–pulse MPP stimulation. The amplitude of each PS at the granule cell layer was measured from the onset to the negative peak. The paired–pulse ratio of the DG population spike was estimated as the ratio of the peak amplitude of the second (PS2) to the first (PS1) population spike following paired–pulse MPP stimulation. The number of the population spikes in each burst evoked by a single stimulus

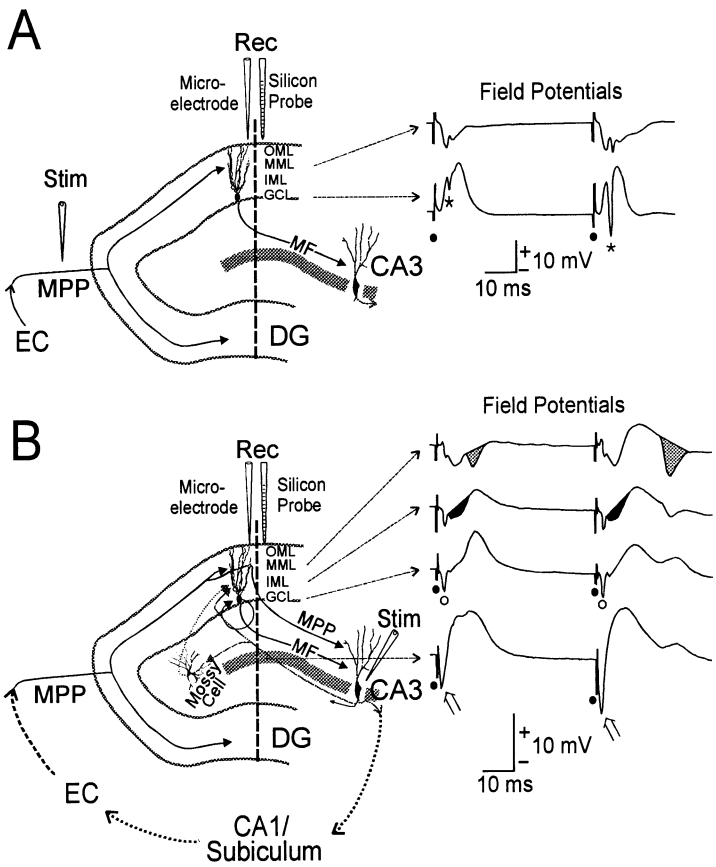

Fig. 1. Schematic diagrams of electrode placement and typical responses. Placement of recording and stimulating electrodes for orthordromic (A) and antidromic (B) stimulation of the DG. (A) Stimulation (Stim) of MPP orthordromically activates the DG resulting in a monosynaptic negative wave in the MML and a population spike (star) in the GCL of the DG (right panel of field potentials). Black filled circles indicate stimulation artifacts. Recording (Rec) was either by a moving microelectrode or a fixed 16-channel silicon probe. (B) Stimulation of mossy fibers at CA3b antidromically activates the DG and CA3c resulting in an antidromic spike in the GCL (open circle) and CA3c pyramidal cells (open arrow), respectively. CA3 stimulation also resulted in negative waves in the IML (black-filled area) and MML of the DG via activation of associational fibers and branching of MPP in CA3, respectively. CA3 stimulation evoked a long-latency negative wave in the MML (dotted area) via the CA3 → CA1/subiculum → EC → MPP → DG loop. Dots indicate the stimulation artifacts.

was counted. Analysis of variance (two-way repeated measures ANOVA followed by Tukey's Protected *t*-test, ANCOVA), a non-parametric Wilcoxon test, paired *t*-test and χ^2 were used for testing statistical significance ($P < 0.05$).

Histology

At the end of each experiment, each stimulating electrode position was marked by a lesion made by passing DC current of 0.5 mA for 1 s (Fig. 2A). The locations of the glass pipette recording electrode, typically placed at the granule cell layer as estimated by electrophysiological criteria (Fig. 1B), were marked by dye ejected from the micropipette by a 5–10-μA anodal current at each location for 10 min. Examples of the dye ejected are shown in Fig. 2C. Recording sites of the silicon probe were not directly verified, but the location of the maximal sink of the DG population spike was considered the landmark of the granule cell layer, as verified by dye ejection from a glass micropipette lowered in the same track as the probe. Under deep anesthesia, the animals were transcardially perfused with 1% buffered sodium sulfide solution (pH 7.4) 100 ml, 1% paraformaldehyde + 1.25% glutaraldehyde solution 100 ml (pH 7.4) and followed by 1% buffered sulfide solution (pH 7.4) 100 ml. The brain was removed and postfixed in 1% paraformaldehyde + 1.25% glutaraldehyde solution for 24 to 48 h. Coronal sections of 40 μm thickness were cut using a cryostat. One set of sections was stained with thionin to verify the electrode placement and cell loss. Another set of sections was processed for modified Timm's sulfide stain[19] to assess MFS (Fig. 2B). Some of these sections were re-stained with thionin. The slides were coated with 0.5% gelatin prior to development. The development was carried out in a solution consisting of 50% w/v gum arabic (120 ml), 20 ml citrate buffer (5.1 g citric acid, 4.7 g sodium citrate), 5.7% hydroquinone (30 ml), and 0.8% silver lactate (30 ml) in a dark water bath at 26°C for 70–90 min. The slides were then rinsed in running tap water for 20–30 min. Some slides were counterstained lightly with thionin, dehydrated, cleared in xylene, and coverslipped with Permount.

Quantification of Timm's stain in the inner molecular layer

The average optical density (OD) of the Timm's stain in the IML of each blade of the DG (dorsal or ventral) was used to quantify the various degrees of MFS caused by KA-seizures. The images of three coronal sections of each rat, within 1 mm from the recording track, were captured by a video camera using a Zeiss Axioskop microscope equipped with a computer-based image system (Northern Eclipse imaging software, ImageExperts, Missisauga, ON). OD was represented as a grey value between white (0) to black (255). The IML and outer 2/3 molecular layer of the DG were respectively outlined and the average grey value within each encircled region was determined by image analysis software (NIH Image; v. 1.57; public domain) for each section. In each section, the difference between the grey value at IML

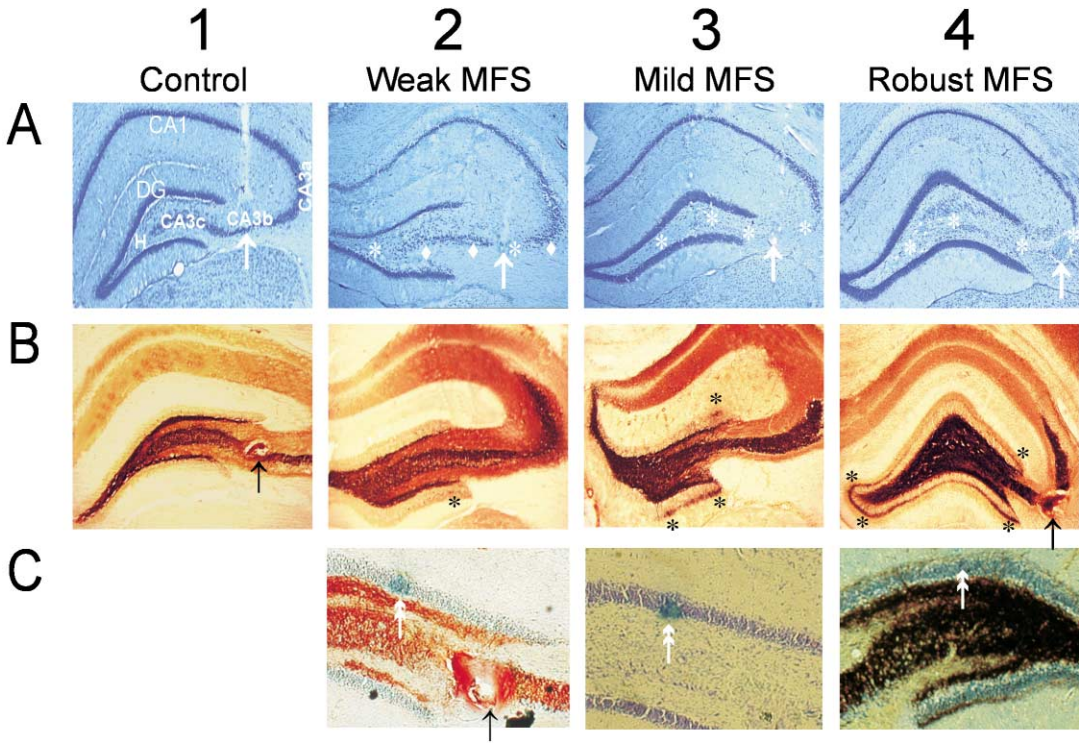

Fig. 2. Examples of MFS and recording tracks. (A, B) Thionin (A) and Timm's (B) stained sections from control (column 1) and KA-treated rats. MFS in the ventral blade of the DG in KA-treated rats was classified as weak, mild and robust (column 2, 3 and 4, respectively). Note that the hilar and CA3 cell loss in weak MFS was not as severe as those in mild MFS or robust MFS (ventral blade of the DG). White stars indicate cell loss, and white diamond in A2 indicates pockets of surviving CA3 cells. Black stars indicate dense positive Timm's stain in the IML of the DG. In the examples shown, positive IML Timm's stain was stronger in the ventral blade than that in the dorsal blade of the DG. No Timm's stain was found in the IML of control rat. White or black arrow indicates the location of the CA3 stimulating electrode. (C) Examples of blue dye (at white arrow with double head) ejected by the micropipette in the granule cell layer of the DG dorsal blade in weak, mild or robust MFS rats. Column 3 is a section with thionin stain only. Columns 2 and 4 are sections with both Timm's and thionin stains; robust MFS was found in the DG ventral blade in column 4.

Table 1. Optical density values of the Timm's stain at the inner molecular layer of both blades of the dentate gyrus in control and kainic acid-treated rats with different degrees of mossy fiber sprouting (MFS)

Group (*n*)	Control (11)	Weak MFS (7)	Mild MFS (13)	Robust MFS (11)
Dorsal blade	18.5 ± 3.2	20.6 ± 3.9	61.2 ± 2.2*	107.9 ± 3.8*
Ventral blade	19.9 ± 1.6	25 ± 2.8	76.5 ± 2.5*	126.2 ± 7.3*

*$P < 0.001$ compared to left groups (Tukey's Protected *t*-test after two-way ANOVA). No significant difference was found for the OD values between the dorsal and ventral blades in each group.

and that at outer 2/3 of the molecular layer was determined for each blade of the DG. For each rat, the average OD of Timm's staining in the IML was taken as the average of the grey value difference for the three sections. An increase in this average OD value was reported to reflect greater MFS in the IML of the DG.[35,44]

RESULTS

Mossy fiber sprouting in the inner molecular layer of the dentate gyrus

KA injection resulted in stage V behavioral seizures in all rats, and about 80% of them developed status epilepticus. About 20% of the rats died. Moderate to severe hilar and CA3 cell loss (Fig. 2A) was found in KA treated rats with different degrees of MFS (Fig. 2B). Therefore, the KA-treated rats were divided into three groups with weak, mild and robust MFS, based initially on visual inspection. The grouping was confirmed by the OD value of the IML Timm's granules in the DG (Table 1). OD values were significantly higher in the robust MFS group than the other groups, and were also significantly higher in the mild MFS group than the weak MFS and control groups, but no statistical difference was found between the control and weak MFS groups. OD values were not statistically different between the dorsal and the ventral blades of the DG (Table 1).

Mossy fiber sprouting in kainic acid-treated rats correlated negatively with the inner molecular sink evoked by CA3 stimulation

Recurrent excitation among granule cells was studied

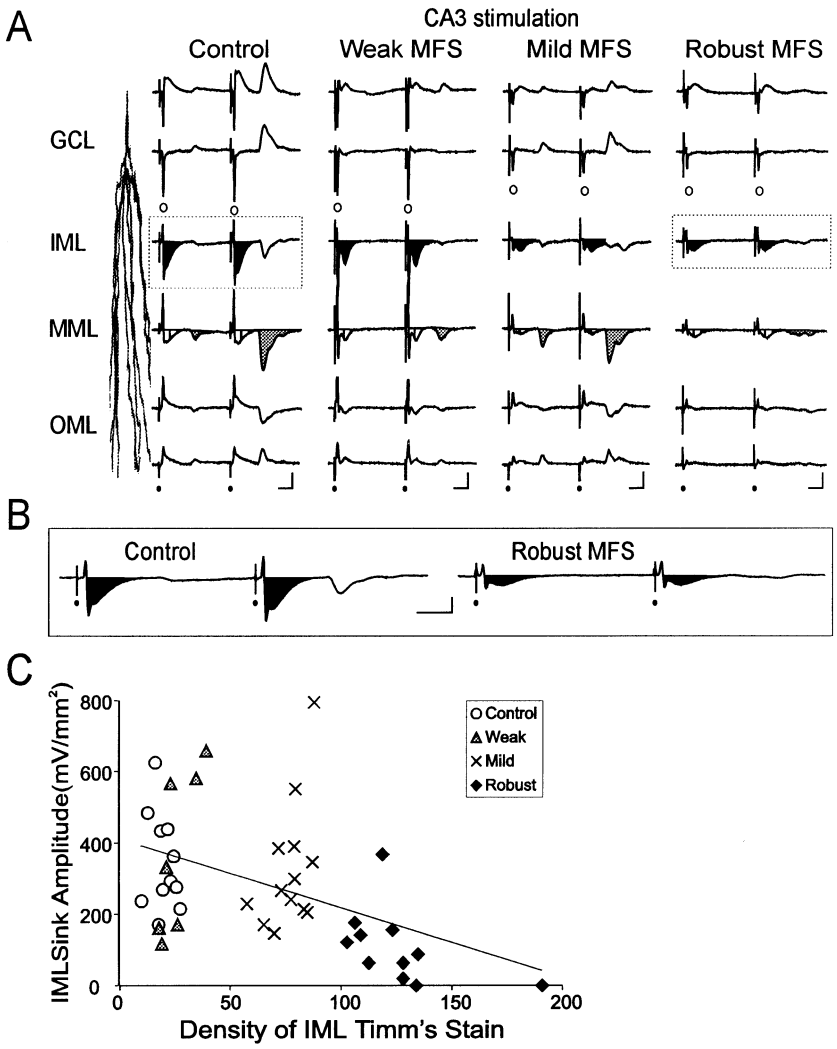

Fig. 3. The increase in MFS correlates negatively with the current sink at the IML activated by CA3/mossy fiber stimulation. (A) CSD time transients at different layers of the ventral blade of the DG following 200 μA CA3 stimulation. The recordings shown correspond to the four rats in the four groups (columns) shown in Fig. 2A and B. A schematic granule cell on the left is labeled with GCL, IML, MML, and OML. Note that the IML sink (black filled area) was smaller in KA-treated rats than the respective measure in control rats. The larger antidromic GC spike at GCL (open circle) in the KA-treated rats with robust MFS only induced a small IML sink. The antidromic spike sink is not significantly different among groups. CA3 stimulation also evoked early (vertical line shaded area) and late MML sink (dotted filled area). The late MML sink was undetectable in the representative robust MFS rat. Black dots indicate stimulation artifact. Scale bar = 10 ms and 500 mV/mm^2. Source is up. (B) The traces as shown in dotted line boxes in A were expanded. (C) A negative correlation exists between the peak amplitude of IML sink following CA3 stimulation and the OD of Timm's stain of the IML in the DG, either dorsal or ventral blade ($r = -0.52$, $P < 0.01$, $n = 42$, df = 40). OD evaluation of Timm's stain was done within 1 mm of the recordings shown.

by backfiring the mossy fibers that coursed through CA3. An antidromic population action potential in the DG was evoked by stimulation of CA3 (stimulus site indicated by 'Stim' in Fig. 1B and by a white arrow in Fig. 2A), confirming activation of the mossy fibers. The latter antidromic spike appeared as a sharp negative wave at the granule cell layer (GCL; open circle in Fig. 1B). CSD analysis revealed a sharp current sink at the GCL during the antidromic spike (downward going transient at open circle in Fig. 3B), accompanied by sharp outward current at the middle and outer molecular layers. Stimulus threshold of the antidromic spike did not differ among control and KA-treated rats. Thus, a fixed stimulus intensity of 200 μA was used in all rats, which evoked an antidromic spike amplitude that was not significantly different among the groups with different degrees of MFS.

The antidromic spike transient was followed by a slow current sink in the IML starting at 2–3 ms, and lasting about 10 ms (black filled area in Fig. 3A, B). This IML sink was accompanied by current sources of a similar duration at the GCL and distal dendrites. There was no correlation between the magnitudes of the antidromic DG spike and the IML sink following CA3 stimulation. Effectively, the IML could be determined electrophysiologically as the depth between the maximal spike sink at the GCL and the maximal EPSP sink at MML following the MPP stimulus. Electrophysiological determination of the GCL was further confirmed by dye injection (Fig. 2C).

Table 2. Peak amplitude of the inner molecular layer sink (mV/mm^2) in both blades of the dentate gyrus following the first pulse of paired–pulse stimulation of CA3 in control and kainic acid-treated rats with different degree of mossy fiber sprouting

Group (n)	Control (11)	Weak MFS (7)	Mild MFS(13)	Robust MFS (11)
Dorsal blade	348 ± 66	336 ± 112	330 ± 49	146 ± 48*
Ventral blade	346 ± 45	370 ± 87	326 ± 50	109 ± 32*

*$P < 0.001$ compared to other groups in the same blade (Tukey's Protected t-test after two-way ANOVA). Similar results were found following the second pulse of CA3 stimulation.

The peak amplitude of the IML sink following CA3 stimulation was significantly smaller in KA-treated rats with robust MFS than any other group (Fig. 3A, B; Table 2). A negative correlation ($r = -0.7$, $P < 0.001$, $n = 32$) was found between the peak amplitude of the IML sink and the optical density of the IML Timm's stain in the same blade of the DG (Fig. 3C). Thus, in contradiction to our initial hypothesis, we observed a decrease in the excitatory sink in the IML in KA-treated rats with robust MFS.

An orthodromic late inner molecular layer sink was decreased in kainic acid-treated rats

In the last section, we inferred no increase of recurrent excitation when the axons of the granule cells were backfired. Since antidromic conduction along axon collaterals is not normal, and it may be blocked at branch points,[42] we also attempted to activate recurrent excitation among granule cells by orthodromic excitation through the MPP.

Stimulation of MPP resulted in a population EPSP that was maximally negative at the MML and a population spike that was maximally negative at the GCL (Fig. 1A).[37,39,67] The mean stimulus threshold for evoking a population EPSP was 10–20 μA, and it did not differ between control and KA-treated rats. The threshold for evoking a visible population spike in the DG was also not statistically different between control (85 ± 9 μA, $n = 32$) and KA-treated (72 ± 8 μA, $n = 31$) rats. Thus, a fixed stimulus intensity of 200 μA was used for evoking responses for CSD analysis.

In 14 out of 27 control rats, MPP stimulation (200 μA) resulted in a late sink in the IML of the DG, presumably through multisynaptic activation of hilar/CA3 cells (Fig. 1B). This late IML sink started at 9.2 ± 0.2 ms latency and lasted over 10 ms (black filled areas in Fig. 4A–D). The late IML sinks were mainly observed in the dorsal blade and occasionally in the ventral blade of the DG as well. This late IML sink in the DG was reliably preceded 2–3 ms earlier by a CA3c population spike (dotted line in Fig. 4). The size of the late IML sink correlated positively with the amplitude of the CA3c spike ($r = 0.7$, $P < 0.001$, $n = 82$, df = 80, Fig. 4E), but not the amplitude of the GC spike ($r = 0.15$, $P = 0.22$, $n = 82$, df = 80) after MPP stimulation. We inferred that hilar/CA3 neurons and the DG are activated in parallel following MPP stimulation, and hilar/CA3 neurons provide a subsequent excitatory feedback to the DG at the IML (Fig. 1B).

The late IML sink following MPP stimulation was found less frequently in KA-treated than control rats. The late IML sink occurred rarely in rats with robust MFS (one out of nine rats, 11%), significantly less frequently (χ^2 (1) = 6, $P < 0.05$) than in control rats (14 out of 27 rats, 52%). The occurrence of the late IML sink in rats with mild MFS (six out of 13 rats, 46%) or weak MFS (two out of seven rats, 29%) was not different from that in control rats.

Effects of CA3 neuronal degeneration in kainic acid-treated rats—decrease in antidromic excitation of the dentate gyrus and recurrent CA3c excitation

Other than backfiring mossy fibers, CA3 stimulation also provided excitation of the DG via the MPP fibers and recurrent excitation of CA3c via axon collaterals.[66] In this section, we reported the decrease in these excitations in KA-treated rats compared to control rats.

An early sink (2–4 ms onset) in the MML of the DG following CA3 stimulation was inferred to result from antidromic stimulation of MPP axons that projected to both DG and CA3.[66] The peak amplitude of this MML sink (vertical line filled areas in Fig. 5) was significantly smaller in each of the three KA-groups than the control group (Table 3), although the onset latency or duration of this sink was not different among KA-treated and control rats. The decreased MML sink in KA-treated rats was likely caused by CA3 cell loss. Because MPP axons synapses in DG before arriving in CA3, stimulation of CA3 would result in DG excitation (at the MML) as shown, and loss of CA3 cells would reduce the latter MML excitation, because fewer MPP axons would be found in CA3.

Recurrent excitation in CA3c after CA3b stimulation in control rats was observed in two ways. First, an antidromic spike was evoked in the CA3c pyramidal cell layer (open arrow in the bottom field potential trace in Fig. 1B and open circle in Fig. 5A). Second, slow sinks (with 2–3 ms onset latency and ~10 ms duration) were found at the dendritic layers on both sides of CA3c cell layer (areas filled with slanted lines in Fig. 5A). We inferred[66] that CA3c neurons were first backfired by CA3b stimulation, which also evoked recurrent excitatory currents at the dendrites of CA3c neurons. Antidromic CA3c spikes and recurrent CA3 dendritic excitation were observed less frequently in KA-treated rats, and they were found respectively in 13% and 38% of KA-treated rats (compared to 100% of control rats). They were not found in two KA-treated rats shown in Fig. 5B and C. Even among rats that showed a distal dendritic

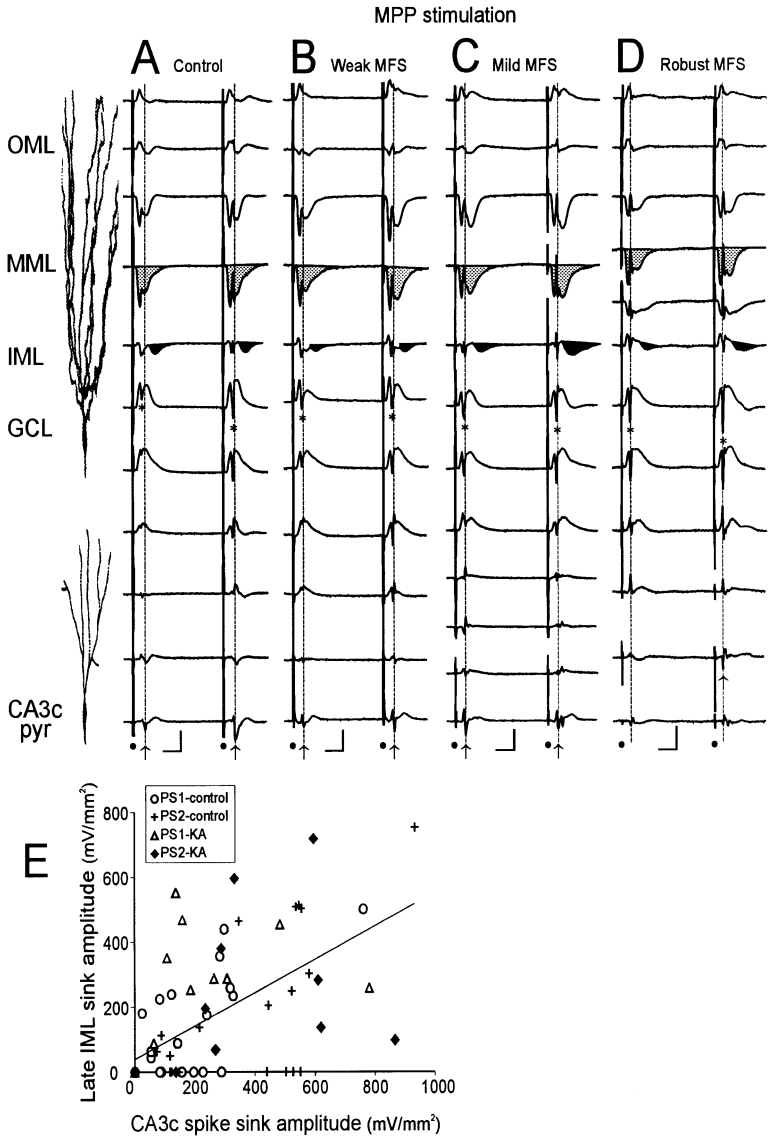

Fig. 4. Late proximal dendritic (inner molecular layer) sink correlated positively to CA3c population spike following MPP stimulation. MPP stimulation of 200 μA evoked a population spike in CA3c, which preceded proximal dendritic excitation of the DG at the IML. CSD time transients in a control (A) and three KA-treated rats with weak MFS (B), mild MFS (C) and robust MFS (D) along the axis of a schematic granule cell and CA3 neuron on the left were shown. The recording track was marked by dye ejection at the GCL, and histology for the rat shown in B is shown in Fig. 2C2. MPP stimulation evoked a population spike (sink) at GCL, labeled with a star, followed by a population spike sink at the CA3c pyramidal cell layer (CA3c pyr), labeled with a solid arrow along a dotted line. MPP stimulation induced the typical excitation (sink) at the MML (gray dotted filled area), followed by a long latency IML sink (black filled area). Scale bars = 10 ms and 1 V/mm^2. Source is up. (E) A positive correlation was found between the IML sink and the amplitude of CA3c population spike sink following either pulse 1 (PS1) or pulse 2 (PS2) of the paired-pulse stimulation of MPP (50 ms IPI) in both KA-treated and control rats ($r = 0.7$, $P < 0.001$, $n = 82$, df = 80).

Table 3. Peak amplitude of middle molecular layer sink (mV/mm^2) in the dorsal blade of the dentate gyrus evoked by the first pulse of paired–pulses applied to medial perforant path or CA3 stimulation in different groups of rats

Group (n)	Control (11)	Weak MFS (7)	Mild MFS(13)	Robust MFS (11)
MPP-stim	1017.3 ± 376	1318.3 ± 289.6	855.2 ± 131.5	718.2 ± 175
CA3-stim	1135.7 ± 65.3	339.4 ± 77.4*	336.9 ± 105.7*	283.2 ± 110.7*

*$P < 0.05$ compared to control group (Tukey's Protected t-test after two-way ANOVA). MPP-stim and CA3-stim represent MPP and CA3 stimulation, respectively. Similar results were found in the ventral blade of the DG.

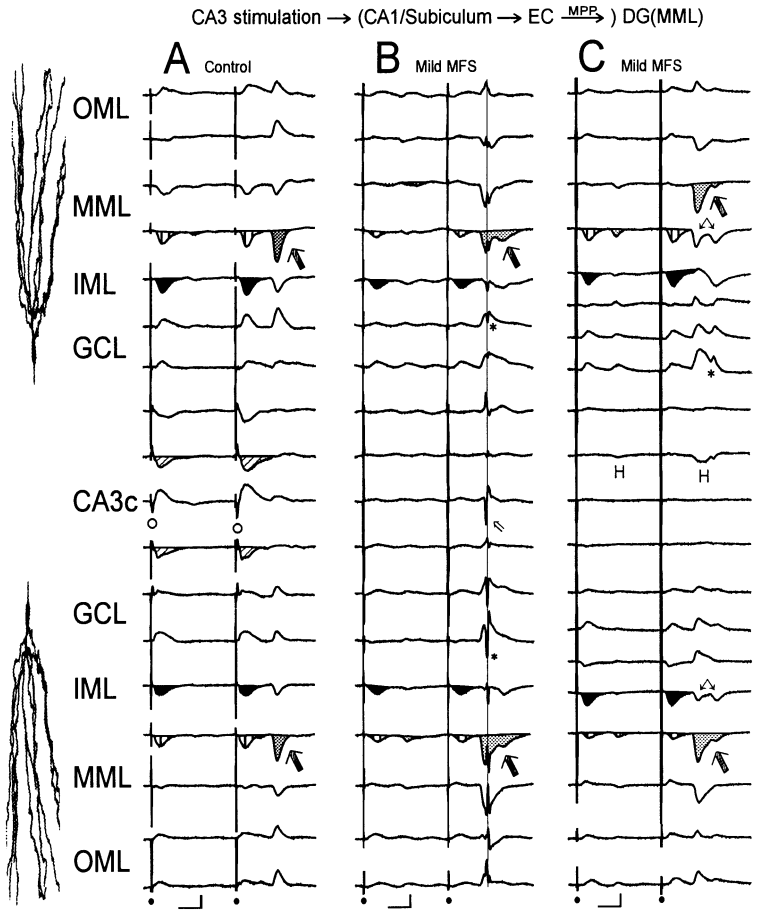

Fig. 5. Enhancement of long-loop activity in the KA-treated rats following CA3 stimulation. CSD time transients at a recording track through both dorsal and ventral DG, following 200 μA CA3 stimulation. (A) A representative control rat showing a long-latency current sink in the MML (stripped arrows, grey shaded area). (B) A mild MFS rat with long latency spike sink in the DG (star) and CA3c (angled hollow arrow); and C, another mild MFS rat with two consecutive long latency sinks in IML-MML (double arrows) and one long latency sink in hilus (marked by H). The histology of the mild MFS rat shown in C is shown in Fig. 2C3. Areas filled with slanted lines in A indicate early dendritic sinks in CA3c or hilus, not found in B and C. Open circle in A indicates antidromic spike in CA3c pyramidal cell layer. Black filled areas indicate early IML sinks. Areas filled with vertical lines indicate early MML sinks. CA3c represents pyramidal cell layer of the CA3c. Black dots indicate stimulation artifact. Scale bars = 10 ms and 500 mV/mm^2. Source is up.

Table 4. Slope of the long-latency current sink (mV/mm^2/ms) at the middle molecular layer of the dorsal blade of the dentate gyrus following the first or the second pulse of a paired–pulse stimulation of CA3 in different groups of rats

	Control (*n*)	Weak MFS (*n*)	Mild MFS (*n*)	Robust MFS (*n*)
Total no.	32	7	13	11
First pulse	83.7 ± 17.2 (16)	87.9 ± 14.9 (5)	113 ± 38.6 (13)	46.2 ± 5.8 (5)
Second pulse	240.6 ± 32.2 (30)	246.9 ± 62.3(7)	437 ± 63.8 (13)*	70.7 ± 20.7 (11)*

*$P < 0.01$ compared to the other groups following the second pulse of CA3 stimulation (Tukey's Protected *t*-test after two-way ANOVA). Similar results were observed in the ventral blade of the dentate gyrus.

sink in CA3c, the amplitude of this sink was significantly smaller in KA-treated than control rats ($P < 0.01$). The decreased CA3c excitation was likely due to CA3c cell loss and axonal degeneration.

Enhancement of the reverberant hippocampo–entorhinal cortex transmission in kainic acid-treated rats

CA3 stimulation was effective in inducing reverberant activity that involved the hippocampus and the entorhinal cortex.[22,66] In this section, this reverberant activity was assessed in KA-treated and control rats. The reverberant activity was manifested as a late sink in the DG, >20 ms latency following CA3 stimulation (grey filled area in Fig. 1B). This late DG sink in the MML (grey filled areas indicated by grey arrow in Fig. 5), accompanied by sources at the GCL and OML, resembled the CSD pattern generated by monosynaptic excitation of the

MPP at the mid-molecular layer of the DG. In fact, the late DG sink was abolished after inactivation/lesion of the MPP[66] or entorhinal cortex (EC).[22] Thus, we suggest a reverberant excitation through a multisynaptic CA3 → CA1/subiculum → EC → DG circuit (Fig. 1B).[66]

The late MML sink was larger for the second than the first pulse in all rats (Table 4). The amplitude of the late MML sink was the highest in the KA-treated with mild MFS group of rats and the smallest in the robust MFS, while weak MFS and control groups showed comparable amplitude. In some KA-treated rats, two or three consecutive long-latency DG sinks with about 8-ms interval between their peaks were evoked by the second pulse of paired CA3 stimulation (branching arrows at MML in Fig. 5C). A long-latency population spike in the DG was found to rise from the late MML sink (dotted area in MML in Fig. 5), mainly following the second pulse of CA3 stimulation. CSD analysis revealed that the late DG spike corresponded to a sharp sink at GCLs of both blades (stars in Fig. 5B). This late DG population spike was found in some KA-treated rats (stars in GCL of Fig. 5B, C), but not in any of the 34 control rats. Among the KA-treated rats, the incidence of long-latency DG spike evoked by CA3 stimulation was significantly higher in the mild MFS group (69%) than in the robust MFS group (18%) [$\chi^2(1) = 6.25$, $P < 0.05$], but not statistically different from the weak MFS group (57%).

A long-latency (>20 ms) EPSP in the CA3c/hilar region after the second pulse of a paired–pulse stimulation of CA3 was found in 24% of the KA-treated rats, but in none of the control rats. The long-latency CA3c/hilar sink was more often located in the CA3c dendritic area close to the dorsal blade of the DG (H in Fig. 5C). A long-latency population spike in the CA3c/hilar region following CA3 stimulation was found to accompany the EPSP in some KA-treated rats. The late population spike corresponded to a sharp sink in the CA3c cell layer (angled hollow arrow in Fig. 5B) and was surrounded by two sources at the CA3c dendritic layers. The late population spike in the CA3c/hilar region was found in 44% of the mild MFS group, 9% of the weak MFS group, and 0% in the robust MFS and control groups. MPP stimulation also evoked long-latency (16–19 ms) MML sink in about 13% of the KA-treated rats but none of the control rats.

Population excitation and inhibition in the dentate gyrus after medial perforant path stimulation

Transmission of the entorhinal cortex to the DG was assessed in KA-treated and control rats by stimulation of the MPP. MPP stimulation evoked a short-latency (1.5–2 ms onset) current sink at the mid-dendrites (MML) of the DG (grey shaded area in Fig. 4A–D), surrounded by distal and proximal sources.[15,37] As determined by micropipette mapping, the magnitude of the MML dendritic sink, evoked by 200 μA stimulus intensity, did not differ significantly among the different groups of KA-treated and control rats (Table 3).

Detailed analyses of the population EPSPs at the MML and population spikes at the GCL of DG were carried out using recordings made simultaneously from a silicon probe. EPSP slope following either the first or the second-pulse (50 ms later) stimulation of MPP was significantly larger in KA-treated than in control rats at stimulus intensities ≥200 μA (Fig. 6A, B). A similar pattern of change was also found for the population spikes in KA-treated rats. The amplitude of the PS1 was significantly larger in the KA-treated than in control rats at MPP stimulus intensities of 80–600 μA (Fig. 6D). The amplitude of PS2 at IPI of 50 ms was also larger in KA-treated than in control rats, but only showed a significant difference at 400–600 μA (Fig. 6E). However, the paired–pulse ratio of the EPSP slopes or the population spikes (PS2/PS1 ratio) was significantly smaller in KA-treated than in control rats (Fig. 6C, F), indicating an increase in paired–pulse inhibition in the DG. We found that the PS2/PS1 ratio was significantly smaller in KA-treated than in control rats at IPIs of 30–100 ms and 200-μA MPP stimulation (Fig. 6G).

When the amplitude of PS2 was plotted as a function of the amplitude of PS1, the curve was downward shifted in KA-treated compared to control rats (Fig. 7A). This indicated that for the same PS1, PS2 at IPI of 50 ms was smaller in KA-treated than in control rats ($P < 0.01$, ANCOVA), and the same result was found using the full range of PS1 amplitudes (Fig. 7A) or a limited range of PS1 (<13 mV in Fig. 7B). Thus, while an increase in PS1 contributed to the suppression of PS2, the small PS2/PS1 ratio in KA-treated rats could not be attributed solely to an increased PS1.

Population spike-EPSP coupling was shown by plotting the population spike amplitude at GCL vs EPSP slope at the MML of the DG. Compared to control rats, the KA-treated rats showed similar PS–EPSP curves at small EPSPs (<2.5 mV/ms), but downward shifted PS–EPSP curves for large EPSPs of 2.5–3 mV/ms, for either the first or the second MPP pulse (Fig. 7 C, D). However, EPSP slopes of >3 mV/ms were found only in KA-treated rats, and they were associated with PS amplitudes of >13 mV not found in control rats.

Low dose bicuculline reveals the fragile inhibition in the dentate gyrus in kainic acid-treated rats

The above data suggested an enhancement of inhibition in KA-treated rats compared to control rats. In order to reveal the functional importance of this enhanced inhibition in KA-treated rats, DG responses were studied after blockade of $GABA_A$ receptor-mediated inhibition by bicuculline.

In the control or KA-treated rats without bicuculline, only a single population spike was evoked in the DG following a MPP stimulus pulse of any intensity. Following i.c.v. injection of 1.5 μl of 20 mM bicuculline (which would give 20 μM bicuculline in the ventricular cerebrospinal fluid if diluted into 1.5 ml of assumed cerebrospinal fluid volume), population spike bursts in the DG were evoked by MPP stimulation in all rats (Fig. 8A). The number of the DG population spike bursts was not statistically different between the control ($n = 6$) and KA-treated rats ($n = 4$) (Fig. 8B). Therefore, there was

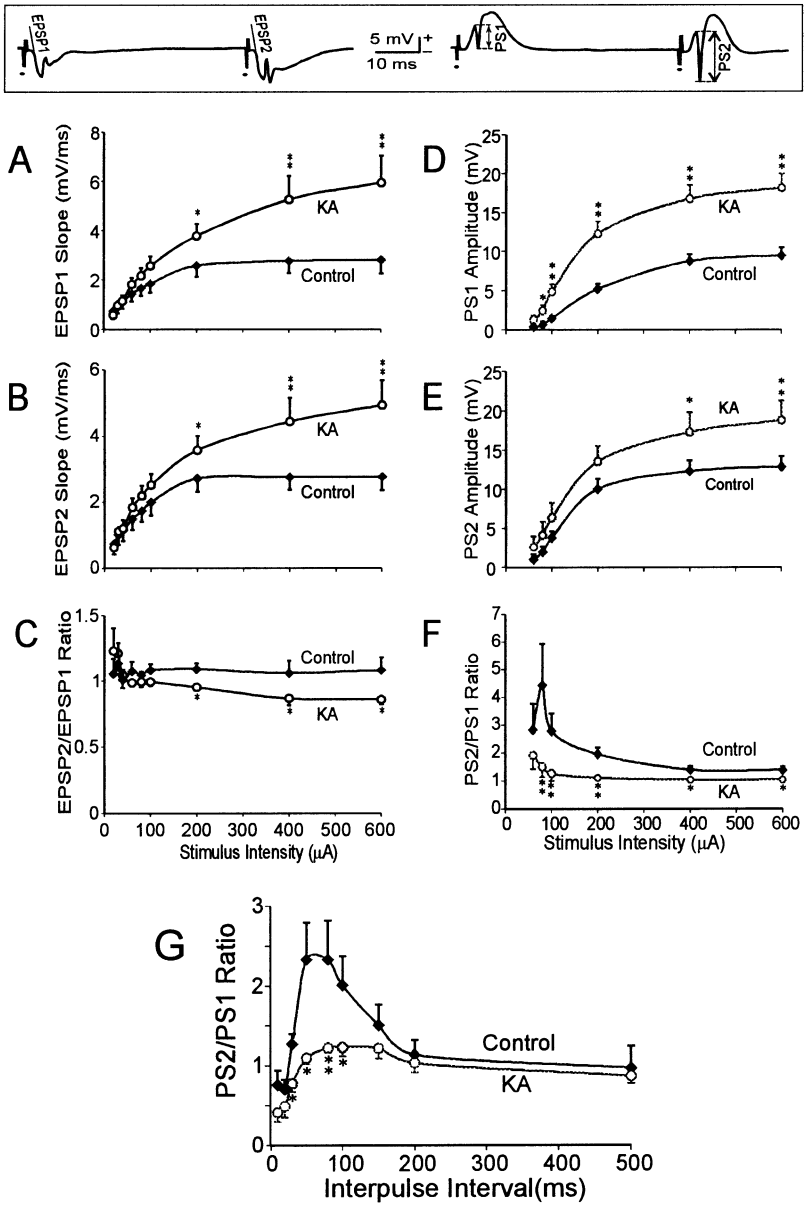

Fig. 6. Paired–pulse inhibition of population EPSP and PS in the DG was increased in KA-treated rats. The slope of the population EPSP at the MML and the amplitude of the PS at the granule cell layer were analysed from average field potentials recorded by a 16-channel silicon probe. Paired–pulses of different stimulus intensities and 50 ms IPI were delivered to the MPP. Insert at top shows measurement of EPSP slope and PS amplitude. The KA-treated rats ($n=9$) consisted of rats with robust ($n=5$) and mild MFS ($n=4$). (A, B) EPSP slope was significantly larger in KA-treated than in control rats ($n=8$) at MPP stimulus intensities $\geq$200 μA of either pulse 1 or pulse 2. (C) EPSP2/EPSP1 ratio was significantly smaller in KA-treated rats than in control rats at MPP stimulus intensities $\geq$200 μA. (D) PS1 amplitude was significantly larger in KA-treated rats than control rats at 80–600 μA of MPP stimulation. (E) PS2 amplitude was significantly larger in KA-treated rats than control rats at 400–600 μA of MPP stimulation. (F) PS2/PS1 ratio following MPP stimulation fixed at 50 ms IPI was significantly decreased in KA-treated rats compared to control rats. (G) PS2/PS1 ratio following stimulation of MPP at 200 μA was significantly decreased at 30–100 ms of IPIs in KA-treated rats compared to control rats. $^{*}P<0.05$, $^{**}P<0.01$ (two-way repeated measures ANOVA followed by post-hoc Tukey's Protected *t*-test).

no detectable difference in DG responses between the KA-treated and control rats after the latter dose of bicuculline, which will be referred to as the high dose.

We found that a smaller dose of bicuculline (1.5 μl of 5 mM, i.c.v., which would dilute to 5 μM bicuculline in the ventricular cerebrospinal fluid) did not induce population spike bursts following MPP stimulation in control rats ($n=7$). We operationally termed this the 'low dose' of bicuculline. In contrast, after a low dose of bicuculline, population spike bursts were evoked by MPP stimulation in all eight KA-treated rats (Fig. 8A, B). Five of the eight KA-treated rats were classified in the mild MFS group and three in the robust MFS group. Responses after bicuculline were not different between

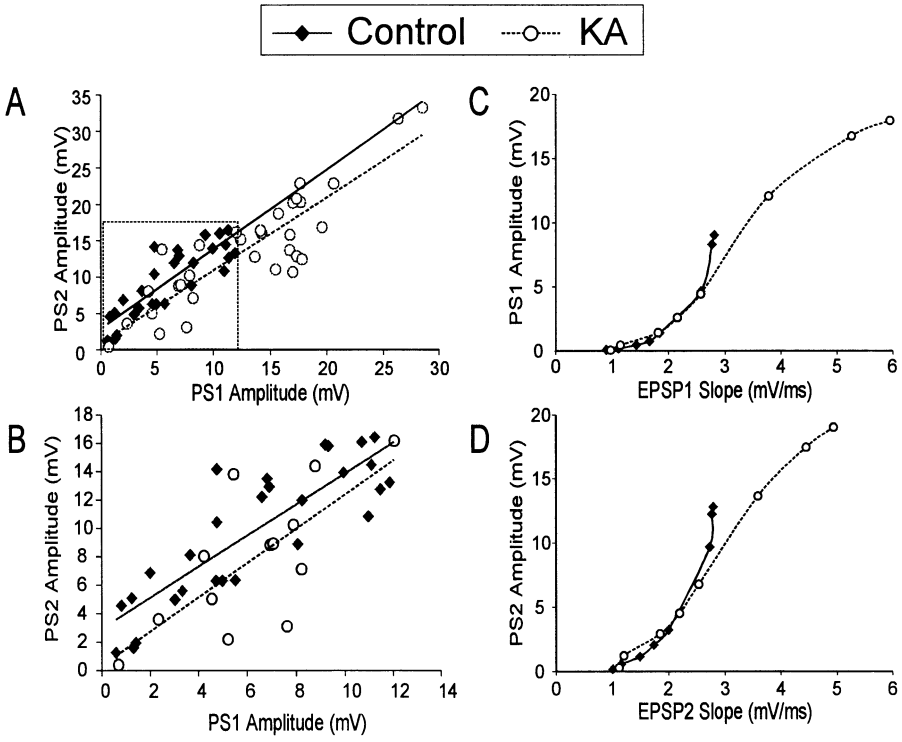

Fig. 7. An increase in inhibition in the DG of KA-treated rats is shown at a fixed PS1 or a fixed population post-synaptic potential. Recordings were made by 16-channel silicon probes from the same groups of rats as Fig. 6, following paired–pulse stimulation of MPP at 50 ms IPI and various intensities. Plot of PS2 vs PS1 illustrated that, for a same PS1, PS2 was significantly decreased in KA-treated rats compared to control rats (A) ($P < 0.05$, ANCOVA). The same pattern was shown in B ($P < 0.05$, ANCOVA) when the data within the dotted line square in A were analysed. Downward shift of the PS amplitude vs EPSP slope curve was found at intermediate EPSPs following either pulse 1 (C) or pulse 2 (D) of MPP stimulation in KA-treated rats compared to control rats, suggesting a decreased spike–EPSP coupling.

the five rats with mild MFS and the three with robust MFS; therefore, these rats were described together.

Similar results were found after CA3 stimulation. After a high dose of bicuculline, population spike bursts in the DG were evoked by CA3 stimulation in both control and KA-treated rats (Fig. 8C). Following a low dose bicuculline, the population spike bursts (≥4 spike peaks) were evoked by CA3 stimulation in all eight KA-treated, but in none of the control rats (Fig. 8C). Excluding the antidromic granule cell (GC) spike, the onset latency of the first spike in the burst after bicuculline was longer than 3 ms following CA3 stimulation. Thus, the population spike bursts were likely mediated by the synaptic activation of the DG following CA3 stimulation.

The bicuculline effects in the DG first affected the MPP-evoked responses at about 7 min post-injection and then affected the CA3-evoked responses at 10–12 min after injection. The effect of bicuculline lasted about 60 min, and the responses usually recovered to baseline levels at about 180 min post-injection. A high dose bicuculline induced spontaneous paroxysmal activity in the DG in control and KA-treated rats (data not shown). Spontaneous paroxysmal activity was also observed in some control and KA-treated rats after a low dose bicucullline (arrows in Fig. 8D).

The IML sink following CA3 stimulation was increased by 27 ± 8% ($n = 4$) in the presence of low-dose bicuculline in the KA-treated rats. However, the amplitude of the IML sink in control rats was not increased (0.1 ± 9%, $n = 4$) after bicuculline.

Paradoxical enhancement of paired–pulse inhibition of population spikes by bicuculline

The low dose of bicuculline paradoxically increased the paired–pulse inhibition of population EPSP and spike in the DG following MPP stimulation in control rats (Figs 8–10). The paired–pulse ratio of the EPSP slopes following MPP stimulation (50 ms IPI) at various intensities was significantly decreased by bicuculline injection (Fig. 9C), although EPSP1 or EPSP2 slope was not significantly changed (Fig. 9A, B). The PS1 amplitude was significantly increased by bicuculline for most MPP stimulus intensities used (Fig. 9D), while the PS2 amplitude at 50 ms IPI and the PS2/PS1 ratio were significantly decreased by bicuculline (Fig. 9E, F).

The plot of PS2 vs PS1 revealed that the amplitude of PS2 at 50 ms IPI was larger before than after low-dose bicuculline for a given PS1 (Fig. 10A). In fact, the PS2 values before bicuculline were mostly above the line of PS2 = PS1, while the PS2 values after bicuculline were all below this line. The plot of PS (at GCL) against EPSP slope (at MML) revealed that the PS1–EPSP1 curve was significantly shifted upwards, while the PS2–EPSP2 curve was shifted downwards at large

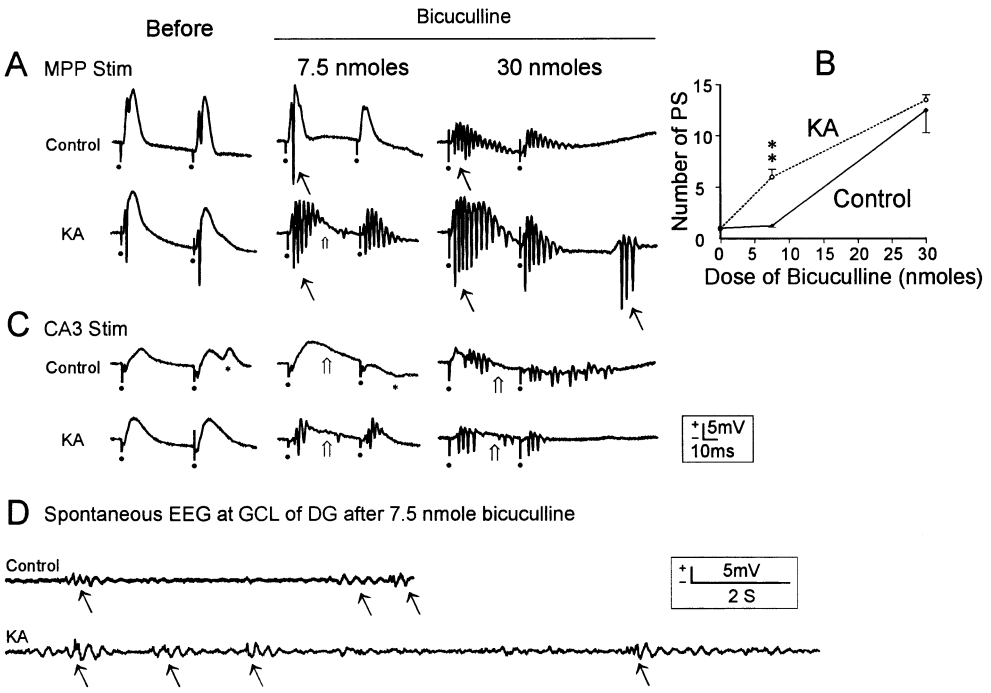

Fig. 8. A low dose of the $GABA_A$ receptor antagonist bicuculline blocked inhibition in the DG in KA-treated but not control rats. Field potentials were recorded by 16-channel silicon probes in representative control and KA-treated rats. (A) Before bicuculline, MPP stimulation (200 μA, 50 ms IPI) evoked a single population spike at GCL of the DG in control and KA-treated rats. After a low dose of bicuculline (1.5 μl of 5 mM or 7.5 nmoles, i.c.v.), the single spike (solid arrow) was increased in amplitude in the control rat but it became a spike burst (solid arrow) in the KA-treated rat. Note that the paired–pulse inhibition was increased after bicuculline in the control rat. Spike bursts were observed in both control and KA-treated rats after a high dose bicuculline (1.5 μl of 20 mM or 30 nmoles, i.c.v.). (B) Dose–response curve revealed that the number of population spikes at the GCL evoked by the first pulse of MPP stimulation was significantly higher in KA-treated rats than in control rats following 7.5 nmoles, but not 30 nmoles of bicuculline (i.c.v.). (C) Field potentials at GCL of the DG following CA3 stimulation (200 μA, 50 ms IPI) in the same rats also showed multiple DG spikes in KA-treated rats but not the control rats after 7.5 nmoles of bicuculline. The 30 nmoles of bicuculline evoked spike bursts in DG in both control and KA-treated rats. Open arrow indicates increased duration of positive waves at GCL after inhibition was blocked by bicuculline. Black dot indicates the stimulation artifact. (D) Spontaneous paroxysmal discharges (indicated by arrows) were shown following 7.5 nmoles of bicuculline in control and KA-treated rats.

EPSPs by bicuculline (Fig. 10B, C). Thus, the low dose of bicuculline decreased tonic inhibition (tested by the first-pulse), but increased evoked inhibition tested by the second-pulse of MPP stimulation. The decrease in PS2/PS1 ratio was also found after bicuculline at IPIs $\leq$ 150 ms (Fig. 10D).

DISCUSSION

The original findings in the present study include: (i) the proximal dendritic (IML) excitation in the DG evoked by CA3 and MPP stimulation was either not changed or decreased after KA seizures. A negative correlation exists between the IML sink and MFS in KA-treated rats, suggesting that increased MFS did not contribute to an increase in IML excitation *in vivo*; (ii) CA3 stimulation evoked a long-latency population spike in the DG and CA3c/hilar region in KA-treated but not control rats, suggesting an enhancement of multisynaptic transmission through the entorhinal–hippocampal loop after seizures; (iii) a low dose of bicuculline paradoxically increased paired–pulse inhibition of DG population spike and EPSPs in control rats; (iv) compensatory increase in paired–pulse inhibition in the DG in KA-treated rats was readily blocked by bicuculline, at a dose that enhanced paired–pulse inhibition in control rats.

Robust mossy fiber sprouting correlates with less inner molecular layer excitation

In a previous study,[66] we have inferred that the IML sink in normal rats following CA3 stimulation was an association fiber mediated excitatory current at the IML. This is confirmed in the present study. The IML sink was strongly attenuated by a non-*N*-methyl-D-aspartate (NMDA) receptor antagonist.[66] Bicuculline did not block the IML sink in normal[66] or control rats, indicating that $GABA_A$ mediated inhibition did not contribute significantly to the IML sink in normal conditions. Population spikes rose from the IML sink under the influence of bicuculline. Thus, the IML sink is likely mediated by inward currents at excitatory synapses in the IML. The outflow of the excitatory currents generates the sources at the GCL and the outer molecular layer (OML). Several studies have shown that excitatory synapses in the IML were formed by afferents of hilar (mossy) cells or CA3c pyramidal cells.[6,11–13,33,38,53,55] The latter excitatory synapses were reduced in KA-treated rats, probably because of hilar

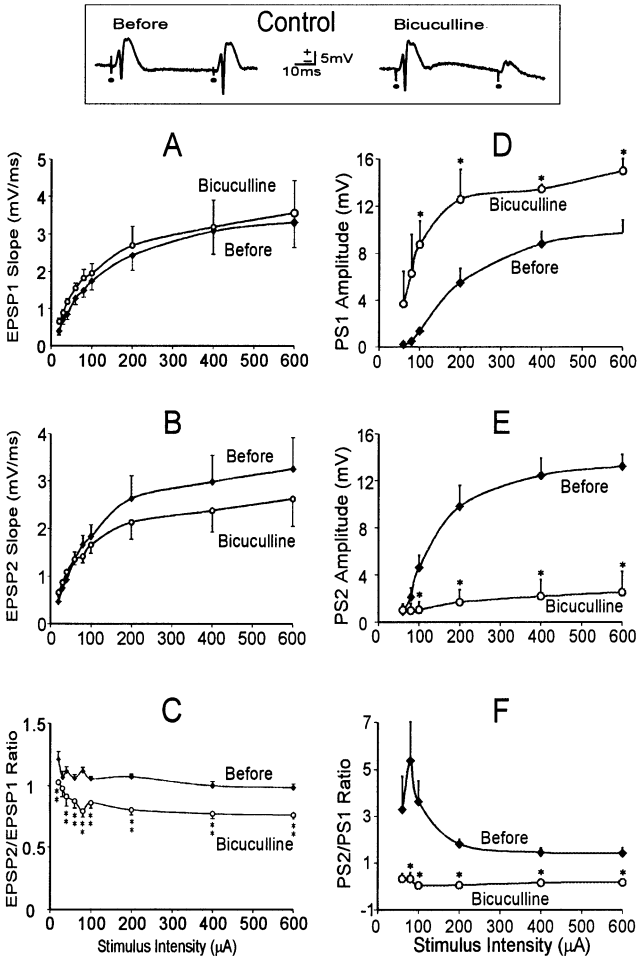

Fig. 9. A low dose of bicuculline paradoxically increased paired–pulse inhibition of DG responses. Paired–pulse inhibition of DG population spike, recorded at the granule cell layer, or population EPSP, recorded at the MML, was paradoxically increased after a low dose of bicuculline (1.5 μl of 5 mM, i.c.v.) in control rats ($n=7$) following stimulation of MPP at 50 ms IPI and various intensities (16-channel silicon probe data). Insert at top shows sample recordings before and after bicuculline in a control rat. (A, B) EPSP slope was not significantly changed by bicuculline. (C) EPSP2/EPSP1 ratio was significantly decreased after bicuculline. (D) PS1 was significantly larger after bicuculline at 100–600 μA of MPP stimulation. (E) PS2 was significant smaller after bicuculline at 100–600 μA of MPP stimulation. (F) PS2/PS1 ratio was significantly decreased after bicuculline at 80–600 μA of MPP stimulation. $^{*}P<0.05$, $^{**}P<0.01$ (two-way repeated measures ANOVA followed by post-hoc Tukey's Protected t-test).

and CA3 cell loss,[10] thus accounting for the smaller IML sink in KA-treated rats. Hilar and/or CA3c cell density was negatively correlated with the IML Timm's stain in KA-treated rats[9] and humans with TLE.[43,43] However, MFS was also observed in seized rats without obvious cell loss.[58]

We found that the IML sink following CA3/mossy fiber stimulation was decreased in KA-treated rats, contrary to our initial hypothesis. This result was found in the group with robust MFS compared to controls (Table 2), and in the negative correlation of the magnitude of the IML sink with the OD index of MFS (Fig. 3C). This result could be explained by an IML sink that was solely mediated by association fiber excitation (above). However, the mossy fibers were clearly activated, as evidenced by the population spike at GCL activated by either antidromic (CA3) or orthodromic (MPP) stimulation, and yet no increase in the IML sink was found in KA-treated rats. This suggests that the stimulus-evoked proximal dendritic recurrent excitation in the DG was relatively weak under normal conditions (without bicuculline). Similar to the IML sink evoked by CA3 stimulation, the orthodromically-activated IML sink following MPP stimulation was also decreased in KA-treated rats compared to control rats, while the amplitude of orthodromic (or antidromic) population spike sink at GCL (preceding the IML sink) was not different between KA-treated and control rats.

Other factors may account for the IML sink decrease after KA treatment. One likely factor is that increased inhibition at the proximal dendrites of granule cells may shunt the recurrent excitation mediated by the mossy fibers and thus reduce the IML sink. Sprouted mossy fibers in the IML were shown to synapse on inhibitory interneurons and GCs,[18,34,57] and sprouting of GABAergic terminals in the IML was found in epileptic animals[20] and patients.[3] The increase in IML sink after blockade of inhibition by bicuculline in KA-treated but not control rats is consistent with the increased inhibitory shunting of

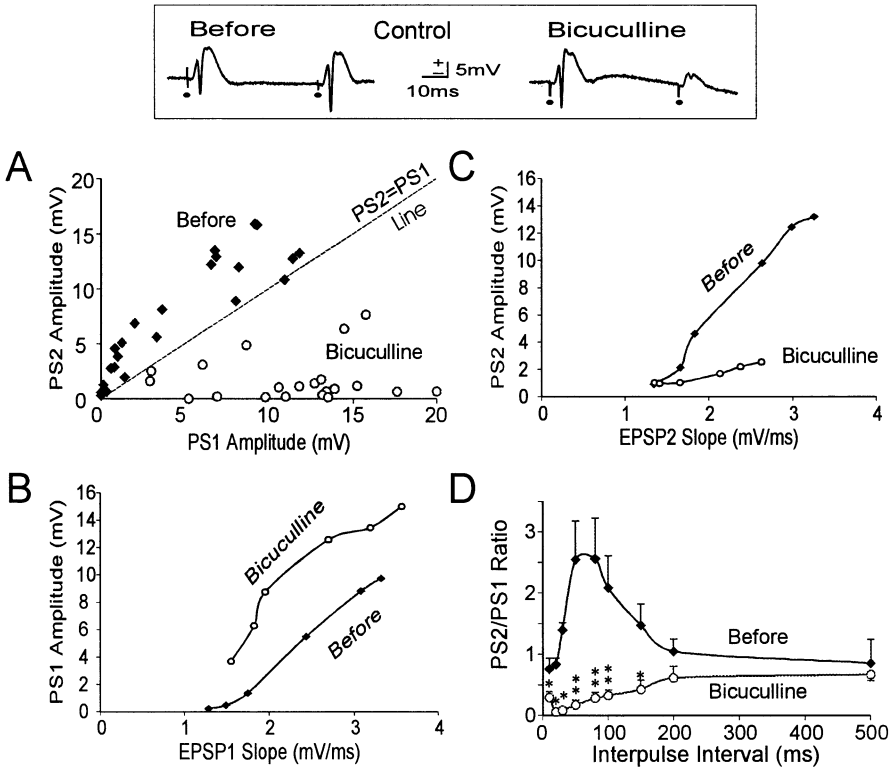

Fig. 10. A low dose of bicuculline changed the relation of the second-pulse population spike (PS1) response in relation to the first-pulse spike in the DG in control rats. Recordings were made by 16-channel silicon probes from the same group of rats as Fig. 9 ($n = 7$). Recordings before and after bicuculline (1.5 μl of 5 mM, i.c.v.) were made in a control rat, as shown in the insert (top). (A) Plot of PS2 vs PS1 illustrated that, for a same PS1, PS2 was smaller after bicuculline injection. Note that the PS2 after bicuculline was shifted downward of the PS2 = PS1 line. (B) Plot of EPSP1 vs PS1 was shifted to left after bicuculline, suggesting a decreased inhibition following the first pulse of MPP stimulation. (C) Rightward shift of the plot of EPSP2 vs PS2 showed that, for a same EPSP2, PS2 was smaller after bicuculline, suggesting an increase in inhibition following the second pulse of MPP stimulation. (D) The ratio of PS2/PS1 following MPP stimulation at 200 μA was significantly decreased by bicuculline at IPIs of 10–150 ms.

the IML sink in KA-treated rats. Additionally, it is possible that sprouting creates axonal branch points which prevent propagation of action potentials beyond these branch points.[42] This would suggest that the sprouted axon collaterals of the mossy fibers normally do not support spike propagation. However, certain pathological conditions, such as an increase in extracellular potassium following neural activity, may promote mossy fiber propagation.

It is possible that the MFS-mediated recurrent excitation is not observed in our rats simply because it was obscured by the large association fiber mediated IML sink *in vivo*. Stimulation of CA3 or the hilus was often used for mossy fiber activation, but the degree of activation of hilar and CA3 cells responsible for the association fibers in IML may be smaller *in vitro*.[66]

The IML sink following MPP stimulation (9–19 ms latency) was rarely found in the robust MFS group of this study. This result differs from that of Golarai and Sutula,[28] who reported that the IML sink (peaking at 9–12 ms latency) after MPP stimulation was only found in kindled rats with MFS (no mossy fiber stimulation was done). However, Golarai and Sutula[28] found another IML sink at 13–16 ms latency in both control and kindled rats. Differences in seizure model and experimental procedures may account for the different results.

Reverberant hippocampo–entorhinal loop was enhanced after kainic-acid seizures

In the mild MFS rats, we found that the long-latency (>20 ms) excitation of the DG following CA3 stimulation was increased, compared to control rats (Fig. 5). The increased EPSP often resulted in a population spike in the DG and CA3c/hilar region. The long-latency DG excitation is likely mediated by a CA3 → CA1/subiculum → EC → DG pathway.[66] Thus, reverberation through this hippocampus–EC loop was enhanced in KA-treated rats, except those with severe CA3 cell loss (robust MFS group). The detailed mechanisms underlying the increased reverberations have not been studied, nor do we know the reason why the reverberations were reduced in the robust MFS group. However, disinhibition and paired-pulse facilitation[17] in the CA1 of KA-treated rats (our unpublished data) would strengthen the reverberations, while cell loss in the entorhinal cortex may suppress them.

'Paradoxical' enhancement of paired–pulse inhibition after low dose bicuculline

Paired–pulse inhibition of the DG population spike was enhanced paradoxically by a low dose of bicuculline (1.5 μl of 5 mM i.c.v.) in control rats (Figs 8–10). It is

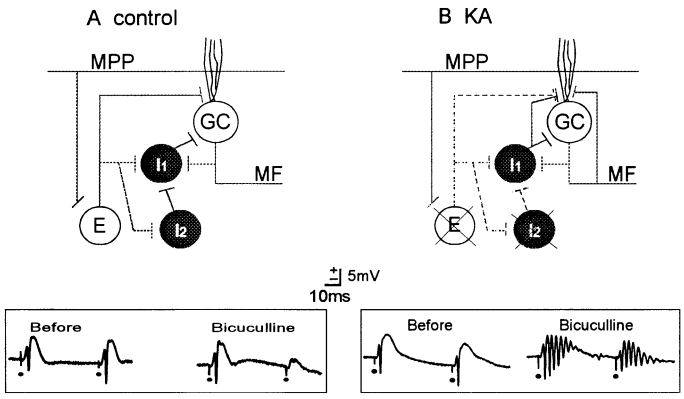

Fig. 11. Model of fragile inhibition in the DG after KA seizures. Insert at bottom shows sample recordings before and after bicuculline in control and KA-treated rats. (A) In control rat, granule cell (GC) receives excitatory inputs from entorhinal cortex via MPP and from hilar excitatory interneuron (E) such as mossy cells, and inhibitory input from inhibitory interneuron (I1). I1 in turn receives excitatory input from mossy fiber collaterals and excitatory interneuron (E), and inhibitory input from I2. MPP stimulation normally resulted in a single population spike in GC with paired–pulse facilitation at 50 ms IPI (before). Bicuculline preferentially blocked I2 input and disinhibited I1 and resulted in increased paired–pulse inhibition of DG population spike (bicuculline). (B) KA treatment resulted in hilar interneuron loss, especially excitatory interneurons (E) like mossy cells and inhibitory interneuron I2, which resulted in disinhibition of I1. Mossy fiber and surviving interneuron sprouting may also change the inhibition and excitation in the DG. MPP stimulation resulted in single population spike with increased paired–pulse inhibition (before). Bicuculline further blocked inhibition of I1 and resulted in bursting of population spike in the DG in KA-treated rats (bicuculline).

inferred that low dose bicuculline blocked tonic inhibition and enhanced PS1. However, it enhanced evoked inhibition of DG granule cells, and decreased PS2. Even when PS1 was matched, PS2 was still smaller after than before bicuculline (Fig. 10A).

A low dose of bicuculline may differentially block inhibitory postsynaptic potentials (IPSPs) on GABAergic interneurons than on principal cells, resulting in more interneuronal excitation and thus a larger inhibition on the dentate granule cells. Zhang *et al.*[69] showed that 10 nM of bicuculline blocked inhibition in GABAergic interneurons but not principal cells *in vitro*. Scharfman[54] reported that bicuculline (10–50 μM) initially increased the evoked IPSPs in the granule cells and suggested a $GABA_A$ receptor-mediated inhibition of IPSPs.

There are similarities in the DG excitability in acute, low-dose bicuculline (in control rats) and chronic, KA treatment (without bicuculline). In each of the two treatments, we found an increase in PS1 (compare Fig. 6D with Fig. 9A), a decreased EPSP2/EPSP1 ratio (Fig. 6C vs Fig. 9C), a decreased PS2/PS1 ratio at $<$100 ms IPI (Fig. 6G vs Fig. 10D), and a rightward shift of the PS2–PS1 curve (Fig. 6B vs Fig. 10A). Differences between the treatments are a larger EPSP enhancement and a less depressed PS2 after KA than bicuculline treatment (Figs 9F, 10D). KA may kill many hilar and other neurons that participate in the GABAergic neuronal interactions (Fig. 11B),[26] inducing an effect functionally similar to that after low-dose bicuculline.[46]

'Fragile inhibition' in the dentate gyrus of kainic acid-treated rats

Paired–pulse inhibition of DG population spikes at $\leq$100 ms IPI was significantly increased in KA-treated rats compared to control rats, confirming previous studies.[9,45] The downward shift of the PS2 vs PS1 curves in KA-treated rats suggests that the feedback inhibition was increased for a given PS1. The decrease in spike-EPSP at a fixed EPSP range also suggests an increase in inhibition, perhaps in an increase in feedback or feed-forward IPSPs in DG granule cells.

Despite the relatively strong inhibition in the DG of KA-treated rats, this inhibition breaks down readily, as shown in this study using a low dose of $GABA_A$ receptor antagonist. This low dose of bicuculline only induced spike bursting in KA-treated but not control rats. We will describe the inhibition in the KA-treated rats as fragile inhibition. The mechanisms underlying this fragile inhibition have not been clearly identified, and they may involve changes in neural circuits rather than only inhibitory synaptic transmission of one type of cells. We suggest that increased inhibition on granule cells in KA-treated rats may be mediated by a decreased inhibition of GABAergic interneurons which the inhibited the granule cells (Fig. 11). In normal rats, a low dose of bicuculline may act to block inhibition in GABAergic interneurons and granule cells, with the interneurons showing a larger blockade. In KA-treated rats, however, the main effect may be blockade of inhibition of granule cells only. Granule cell disinhibition allows paroxysmal spiking during synaptic excitation induced by MPP or CA3 stimulation. Although we detected no increase in recurrent excitation following mossy fiber activation, it is still possible that mossy fiber collaterals may release Zn^{2+} and contribute to an extrasynaptic inhibition breakdown. Recurrent excitation of the proximal dendrites following MPP stimulation is not a likely explanation of the evoked spike bursts because the bursts started at $<$8 ms while the onset of the late IML sink was at $>$9 ms (Results). The changes of intrinsic electrophysiological properties

of granule cells such as decreased spike firing adaptation[24] may also increase the tendency of granule cells to burst.

Altered inhibition in the DG has been reported for several seizure models *in vitro*. GABA-mediated currents were enhanced in the DG following kindling[49] or pilocarpine seizures.[27] However, these currents were less potentiated by benzodiazepine and more suppressed by Zn^{2+},[14] probably because of changes in the GABA-ergic receptor.[7] A low dose of bicuculline was also found to induce multiple spikes in the DG following hilar stimulation in hippocampal slices derived from human TLE[24,43] and KA-treated rats.[18,50] In particular, our findings paralleled the *in vitro* results of Cronin *et al.*[18] in that field responses appeared normal in KA-treated rats with strong MFS until the addition of bicuculline. However, after a low dose of bicuculline, all eight rats with modest or robust MFS showed population spike bursts following CA3 stimulation *in vivo*, while only 44% of the slices showed epileptiform spike bursts *in vitro*.[18]

Inhibition in the DG appears to be increased in TLE patients,[23,32,60,65] although these patients are still more prone to seizures than other subjects. Cortical inhibition is subjected to change with arousal,[16] stress[51,70] or menstruation.[4] These disinhibitory changes may affect excitability in seizure-prone[52,62] but not normal subjects. Thus, the concept of 'fragile inhibition' describes the vulnerability of the compensatory inhibition in the brain in animals and humans with temporal lobe seizures.[48]

Acknowledgements—This work was supported by operating grants from the Medical Research Council MOP-36421 and the Natural Sciences and Engineering Research Council of Canada, and doctoral studentships to K.W. funded by Savoy Foundation and Epilepsy Canada. The multi-channel silicon probes were provided by the Michigan Center for Neural Communication Technology, sponsored by NIH/NCRR grant P41 RR09754-04.

REFERENCES

1. Amaral D. G. and Witter M. P. (1989) The three-dimensional organization of the hippocampal formation: a review of anatomical data. *Neuroscience* **31,** 571–591.
2. Babb T. L., Kupfer W. R., Pretorius J. K., Crandall P. H. and Levesque M. F. (1991) Synaptic reorganization by mossy fibers in human epileptic fascia dentata. *Neuroscience* **42,** 351–363.
3. Babb T. L., Pretorius J. K., Kupfer W. R. and Crandall P. H. (1989) Glutamate decarboxylase-immunoreactive neurons are preserved in human epileptic hippocampus. *J. Neurosci.* **9,** 2562–2574.
4. Becker D., Creutzfeldt O. D., Schwibbe M. and Wuttke W. (1982) Changes in physiological, EEG and psychological parameters in women during the spontaneous menstrual cycle and following oral contraceptives. *Psychoneuroendocrinology* **7,** 75–90.
5. Bekenstein J. W. and Lothman E. W. (1993) Dormancy of inhibitory interneurons in a model of temporal lobe epilepsy. *Science* **259,** 97–100.
6. Bragin A., Csicsvari J., Penttonen M. and Buzsaki G. (1997) Epileptic afterdischarge in the hippocampal-entorhinal system: current source density and unit studies. *Neuroscience* **76,** 1187–1203.
7. Brooks-Kayal A. R., Shumate M. D., Jin H., Rikhter T. Y. and Coulter D. A. (1998) Selective changes in single cell GABA(A) receptor subunit expression and function in temporal lobe epilepsy. *Nat. Med.* **4,** 1166–1172.
8. Buckmaster P. S. and Dudek F. E. (1997) Network properties of the dentate gyrus in epileptic rats with hilar neuron loss and granule cell axon reorganization. *J. Neurophysiol.* **77,** 2685–2696.
9. Buckmaster P. S. and Dudek F. E. (1997) Neuron loss, granule cell axon reorganization, and functional changes in the dentate gyrus of epileptic kainate-treated rats. *J. comp. Neurol.* **385,** 385–404.
10. Buckmaster P. S. and Jongen-Relo A. L. (1999) Highly specific neuron loss preserves lateral inhibitory circuits in the dentate gyrus of kainate-induced epileptic rats. *J. Neurosci.* **19,** 9519–9529.
11. Buckmaster P. S. and Schwartzkroin P. A. (1994) Hippocampal mossy cell function: a speculative view. *Hippocampus* **4,** 393–402.
12. Buckmaster P. S., Strowbridge B. W., Kunkel D. D., Schmiege D. L. and Schwartzkroin P. A. (1992) Mossy cell axonal projections to the dentate gyrus molecular layer in the rat hippocampal slice. *Hippocampus* **2,** 349–362.
13. Buckmaster P. S., Wenzel H. J., Kunkel D. D. and Schwartzkroin P. A. (1996) Axon arbors and synaptic connections of hippocampal mossy cells in the rat *in vivo*. *J. comp. Neurol.* **366,** 271–292.
14. Buhl E. H., Otis T. S. and Mody I. (1996) Zinc-induced collapse of augmented inhibition by GABA in a temporal lobe epilepsy model. *Science* **271,** 369–373.
15. Canning K. J., Wu K., Peloquin P., Kloosterman F. and Leung L. S. (2000) Physiology of the parahippocampal projections to the hippocampus studied by current source density analysis. *Ann. N. Y. Acad. Sci.* **911,** 55–72.
16. Cao F. and Leung L. S. (1991) Behavior-dependent paired-pulse responses in the hippocampal CA1 region. *Expl Brain Res.* **87,** 553–561.
17. Cornish S. M. and Wheal H. V. (1989) Long-term loss of paired pulse inhibition in the kainic acid-lesioned hippocampus of the rat. *Neuroscience* **28,** 563–571.
18. Cronin J., Obenaus A., Houser C. R. and Dudek F. E. (1992) Electrophysiology of dentate granule cells after kainate-induced synaptic reorganization of the mossy fibers. *Brain Res.* **573,** 305–310.
19. Danscher G. (1981) Histochemical demonstration of heavy metals. A revised version of the sulphide silver method suitable for both light and electronmicroscopy. *Histochemistry* **71,** 1–16.
20. Davenport C. J., Brown W. J. and Babb T. L. (1990) Sprouting of GABAergic and mossy fiber axons in dentate gyrus following intrahippocampal kainate in the rat. *Expl Neurol.* **109,** 180–190.
21. de Lanerolle N. C., Kim J. H., Robbins R. J. and Spencer D. D. (1989) Hippocampal interneuron loss and plasticity in human temporal lobe epilepsy. *Brain Res.* **495,** 387–395.
22. Deadwyler S. A., West J. R., Cotman C. W. and Lynch G. (1975) Physiological studies of the reciprocal connections between the hippocampus and entorhinal cortex. *Expl Neurol.* **49,** 35–57.
23. Engel J. Jr (1995) Inhibitory mechanisms of epileptic seizure generation. *Adv. Neurol.* **67,** 157–171.
24. Franck J. E., Pokorny J., Kunkel D. D. and Schwartzkroin P. A. (1995) Physiologic and morphologic characteristics of granule cell circuitry in human epileptic hippocampus. *Epilepsia* **36,** 543–558.
25. Freeman J. A. and Nicholson C. (1975) Experimental optimization of current source-density technique for anuran cerebellum. *J. Neurophysiol.* **38,** 369–382.
26. Freund T. F. and Buzsaki G. (1996) Interneurons of the hippocampus. *Hippocampus* **6,** 347–470.
27. Gibbs J. W. III, Shumate M. D. and Coulter D. A. (1997) Differential epilepsy-associated alterations in postsynaptic GABA(A) receptor function in dentate granule and CA1 neurons. *J. Neurophysiol.* **77,** 1924–1938.

28. Golarai G. and Sutula T. P. (1996) Functional alterations in the dentate gyrus after induction of long-term potentiation, kindling, and mossy fiber sprouting. *J. Neurophysiol.* **75,** 343–353.
29. Haas K. Z., Sperber E. F., Moshe S. L. and Stanton P. K. (1996) Kainic acid-induced seizures enhance dentate gyrus inhibition by down-regulation of GABA(B) receptors. *J. Neurosci.* **16,** 4250–4260.
30. Heinemann U., Beck H., Dreier J. P., Ficker E., Stabel J. and Zhang C. L. (1992) The dentate gyrus as a regulated gate for the propagation of epileptiform activity. *Epilepsy Res. Suppl.* **7,** 273–280.
31. Houser C. R., Miyashiro J. E., Swartz B. E., Walsh G. O., Rich J. R. and Delgado-Escueta A. V. (1990) Altered patterns of dynorphin immunoreactivity suggest mossy fiber reorganization in human hippocampal epilepsy. *J. Neurosci.* **10,** 267–282.
32. Isokawa-Akesson M., Wilson C. L. and Babb T. L. (1989) Inhibition in synchronously firing human hippocampal neurons. *Epilepsy Res.* **3,** 236–247.
33. Jackson M. B. and Scharfman H. E. (1996) Positive feedback from hilar mossy cells to granule cells in the dentate gyrus revealed by voltage-sensitive dye and microelectrode recording. *J. Neurophysiol.* **76,** 601–616.
34. Kotti T., Riekkinen P. J. Sr and Miettinen R. (1997) Characterization of target cells for aberrant mossy fiber collaterals in the dentate gyrus of epileptic rat. *Expl Neurol.* **146,** 323–330.
35. Leite J. P., Babb T. L., Pretorius J. K., Kuhlman P. A., Yeoman K. M. and Mathern G. W. (1996) Neuron loss, mossy fiber sprouting, and interictal spikes after intrahippocampal kainate in developing rats. *Epilepsy Res.* **26,** 219–231.
36. Leung L. S. (1990) Field potentials in the central nervous system-recording, analysis and modeling. In *Neurophysiological techniques. Applications to neural systems* (eds Boulton A. A., Baker G. B. and Vanderwolf C. H.), Vol. 15, pp. 313–369. Humana, Clifton, NJ.
37. Leung L. S., Roth L. and Canning K. J. (1995) Entorhinal inputs to hippocampal CA1 and dentate gyrus in the rat: a current-source-density study. *J. Neurophysiol.* **73,** 2392–2403.
38. Li X. G., Somogyi P., Ylinen A. and Buzsaki G. (1994) The hippocampal CA3 network: an *in vivo* intracellular labeling study. *J. comp. Neurol.* **339,** 181–208.
39. Lomo T. (1971) Patterns of activation in a monosynaptic cortical pathway: the perforant path input to the dentate area of the hippocampal formation. *Expl Brain Res.* **12,** 18–45.
40. Lopes da Silva F. H., Witter M. P., Boeijinga P. H. and Lohman A. H. (1990) Anatomic organization and physiology of the limbic cortex. *Physiol. Rev.* **70,** 453–511.
41. Lothman E. W., Stringer J. L. and Bertram E. H. (1992) The dentate gyrus as a control point for seizures in the hippocampus and beyond. *Epilepsy Res. Suppl.* **7,** 301–313.
42. Luscher H. R. (1998) Control of action potential invasion into terminal arborizations. In *Presynaptic inhibition and neural control.* (eds Rudomin R., Romo R. and Mendell L.), pp. 126–137. Oxford University Press, Oxford.
43. Masukawa L. M., Uruno K., Sperling M., O'Connor M. J. and Burdette L. J. (1992) The functional relationship between antidromically evoked field responses of the dentate gyrus and mossy fiber reorganization in temporal lobe epileptic patients. *Brain Res.* **579,** 119–127.
44. Mathern G. W., Price G., Rosales C., Pretorius J. K., Lozada A. and Mendoza D. (1998) Anoxia during kainate status epilepticus shortens behavioral convulsions but generates hippocampal neuron loss and supragranular mossy fiber sprouting. *Epilepsy Res.* **30,** 133–151.
45. Milgram N. W., Yearwood T., Khurgel M., Ivy G. O. and Racine R. (1991) Changes in inhibitory processes in the hippocampus following recurrent seizures induced by systemic administration of kainic acid. *Brain Res.* **551,** 236–246.
46. Misgeld U. and Frotscher M. (1986) Postsynaptic-GABAergic inhibition of non-pyramidal neurons in the guinea-pig hippocampus. *Neuroscience* **19,** 193–206.
47. Mitzdorf U. (1985) Current source-density method and application in cat cerebral cortex: investigation of evoked potentials and EEG phenomena. *Physiol. Rev.* **65,** 37–100.
48. Nadler J. V., Perry B. W. and Cotman C. W. (1978) Intraventricular kainic acid preferentially destroys hippocampal pyramidal cells. *Nature* **271,** 676–677.
49. Otis T. S., De Koninck Y. and Mody I. (1994) Lasting potentiation of inhibition is associated with an increased number of gamma-aminobutyric acid type A receptors activated during miniature inhibitory postsynaptic currents. *Proc. natn. Acad. Sci. USA* **91,** 7698–7702.
50. Patrylo P. R. and Dudek F. E. (1998) Physiological unmasking of new glutamatergic pathways in the dentate gyrus of hippocampal slices from kainate-induced epileptic rats. *J. Neurophysiol.* **79,** 418–429.
51. Purdy R. H., Morrow A. L., Moore P. H. Jr and Paul S. M. (1991) Stress-induced elevations of gamma-aminobutyric acid type A receptor-active steroids in the rat brain. *Proc. natn. Acad. Sci. USA* **88,** 4553–4557.
52. Rosciszewska D. (1980) Analysis of seizure dispersion during menstrual cycle in women with epilepsy. *Monogr. Neural Sci.* **5,** 280–284.
53. Scharfman H. E. (1994) EPSPs of dentate gyrus granule cells during epileptiform bursts of dentate hilar 'mossy' cells and area CA3 pyramidal cells in disinhibited rat hippocampal slices. *J. Neurosci.* **14,** 6041–6057.
54. Scharfman H. E. (1994) Paradoxical enhancement by bicuculline of dentate granule cell IPSPs evoked by fimbria stimulation in rat hippocampal slices. *Neurosci. Lett.* **168,** 29–33.
55. Scharfman H. E. (1995) Electrophysiological evidence that dentate hilar mossy cells are excitatory and innervate both granule cells and interneurons. *J. Neurophysiol.* **74,** 179–194.
56. Sloviter R. S. (1987) Decreased hippocampal inhibition and a selective loss of interneurons in experimental epilepsy. *Science* **235,** 73–76.
57. Sloviter R. S. (1992) Possible functional consequences of synaptic reorganization in the dentate gyrus of kainate-treated rats. *Neurosci. Lett.* **137,** 91–96.
58. Stringer J. L., Agarwal K. S. and Dure L. S. (1997) Is cell death necessary for hippocampal mossy fiber sprouting? *Epilepsy Res.* **27,** 67–76.
59. Sutula T., Cascino G., Cavazos J., Parada I. and Ramirez L. (1989) Mossy fiber synaptic reorganization in the epileptic human temporal lobe. *Ann. Neurol.* **26,** 321–330.
60. Swanson T. H., Sperling M. R. and O'Connor M. J. (1998) Strong paired pulse depression of dentate granule cells in slices from patients with temporal lobe epilepsy. *J. neural Transm.* **105,** 613–625.
61. Tauck D. L. and Nadler J. V. (1985) Evidence of functional mossy fiber sprouting in hippocampal formation of kainic acid-treated rats. *J. Neurosci.* **5,** 1016–1022.
62. Temkin N. R. and Davis G. R. (1984) Stress as a risk factor for seizures among adults with epilepsy. *Epilepsia* **25,** 450–456.
63. Tuff L. P., Racine R. J. and Adamec R. (1983) The effects of kindling on GABA-mediated inhibition in the dentate gyrus of the rat. I. Paired-pulse depression. *Brain Res.* **277,** 79–90.
64. Williamson A., Patrylo P. R. and Spencer D. D. (1999) Decrease in inhibition in dentate granule cells from patients with medial temporal lobe epilepsy. *Ann. Neurol.* **45,** 92–99.
65. Wilson C. L., Khan S. U., Engel J. Jr, Isokawa M., Babb T. L. and Behnke E. J. (1998) Paired pulse suppression and facilitation in human epileptogenic hippocampal formation. *Epilepsy Res.* **31,** 211–230.
66. Wu K., Canning K. J. and Leung L. S. (1998) Functional interconnections between CA3 and the dentate gyrus revealed by current source density analysis. *Hippocampus* **8,** 217–230.

67. Wu K. and Leung L. S. (1998) Monosynaptic activation of CA3 by the medial perforant path. *Brain Res.* **797,** 35–41.
68. Wuarin J. P. and Dudek F. E. (1996) Electrographic seizures and new recurrent excitatory circuits in the dentate gyrus of hippocampal slices from kainate-treated epileptic rats. *J. Neurosci.* **16,** 4438–4448.
69. Zhang Y., Perez Velazquez J. L., Tian G. F., Wu C. P., Skinner F. K., Carlen P. L. and Zhang L. (1998) Slow oscillations (= 1 Hz) mediated by GABAergic interneuronal networks in rat hippocampus. *J. Neurosci.* **18,** 9256–9268.
70. Zinder O. and Dar D. E. (1999) Neuroactive steroids: their mechanism of action and their function in the stress response. *Acta physiol. scand.* **167,** 181–188.

(*Accepted* 14 *January* 2001)